LETTER

doi:10.1038/nature09526

Selective activation of p53-mediated tumour suppression in high-grade tumours

Melissa R. Junttila[1]†, Anthony N. Karnezis[1], Daniel Garcia[1], Francesc Madriles[2], Roderik M. Kortlever[1], Fanya Rostker[1], Lamorna Brown Swigart[1], David M. Pham[3], Youngho Seo[3], Gerard I. Evan[1]† & Carla P. Martins[1]†

Non-small cell lung carcinoma (NSCLC) is the leading cause of cancer-related death worldwide, with an overall 5-year survival rate of only 10–15%[1]. Deregulation of the Ras pathway is a frequent hallmark of NSCLC, often through mutations that directly activate Kras[2]. p53 is also frequently inactivated in NSCLC and, because oncogenic Ras can be a potent trigger of p53 (ref. 3), it seems likely that oncogenic Ras signalling has a major and persistent role in driving the selection against p53. Hence, pharmacological restoration of p53 is an appealing therapeutic strategy for treating this disease[4]. Here we model the probable therapeutic impact of p53 restoration in a spontaneously evolving mouse model of NSCLC initiated by sporadic oncogenic activation of endogenous Kras[5]. Surprisingly, p53 restoration failed to induce significant regression of established tumours, although it did result in a significant decrease in the relative proportion of high-grade tumours. This is due to selective activation of p53 only in the more aggressive tumour cells within each tumour. Such selective activation of p53 correlates with marked upregulation in Ras signal intensity and induction of the oncogenic signalling sensor p19^{ARF} (ref. 6). Our data indicate that p53-mediated tumour suppression is triggered only when oncogenic Ras signal flux exceeds a critical threshold. Importantly, the failure of low-level oncogenic Kras to engage p53 reveals inherent limits in the capacity of p53 to restrain early tumour evolution and in the efficacy of therapeutic p53 restoration to eradicate cancers.

Inactivation of the p53 (also known as Trp53) tumour suppressor pathway is a common feature of human cancers, fostering the attractive notion of restoring p53 function in established tumours as an effective and tumour-specific therapeutic strategy[4]. Indeed, p53 restoration was recently shown to trigger dramatic tumour regression *in vivo*[7–9]. Although encouraging, these studies used tumour models (either transgene[7,9] or radiation-induced[8]) driven by preternaturally high levels of oncogenes. Because high-level oncogene activity potently engages p53 via the p19^{ARF} tumour suppressor[6,7,10], p53 restoration has a marked impact in these models. Unlike high oncogenic activity, however, low-level expression of dominant oncogenes seems insufficient to engage intrinsic tumour suppression, even though it still suffices to drive tumorigenesis[11,12]. This raises the spectre that many epithelial malignancies, initiated as they are by low-level oncogenic signals such as those arising from mutational activation of *ras* genes *in situ*, may be insensitive to p53 restoration—at least during certain phases of their evolution. To investigate this possibility we assessed the ability of p53 restoration to trigger tumour regression in the well-characterized *Lox-Stop-Lox-Kras^{G12D}* (*KR*) murine tumour model of NSCLC[5] wherein tumorigenesis is driven by sporadic, low-level activation of mutant Kras. This model closely recapitulates its human disease counterpart[13].

After inhalation of adenovirus-Cre, *KR* mice develop multiple, independently evolving lung tumours, permitting contemporaneous analysis of different disease stages within each animal. *KR* mice were crossed into the *p53$^{KI/KI}$* switchable mouse model in which both alleles of the endogenous *p53* gene are replaced by the conditional variant *p53ER^{TAM}* (ref. 14). *p53$^{KI/KI}$* mice can be reversibly toggled *in vivo* between p53 wild-type and p53 null states by administration or withdrawal of tamoxifen (Tam). Importantly, once functionally restored in Tam-treated *p53$^{KI/KI}$* mice, p53-mediated tumour suppression is triggered only if p53-activating signals are present[7,10].

Kras^{G12D} was sporadically activated in *KR;p53$^{KI/+}$* and *KR;p53$^{KI/KI}$* lungs and tumours were allowed to develop for 16 weeks. In both genotypes, Kras^{G12D} activation induced a spectrum of lung tumour grades including hyperplasias, adenomas and adenocarcinomas. Like *KR;p53*-deficient animals[15] (Supplementary Fig. 1), *KR;p53$^{KI/KI}$* mice show accelerated tumour progression and increased incidence of high-grade tumours relative to their *KR;p53$^{KI/+}$* counterparts. These data affirm that p53 restrains Kras-driven NSCLC yet indicate that, even when combined, Kras^{G12D} activation and p53 inactivation are insufficient to generate malignant tumours without additional, aleatory mutations.

To ascertain its therapeutic impact, p53 function was restored for 1 week in *KR;p53$^{KI/KI}$* lung tumours (Fig. 1a). Surprisingly, given the marked tumour regression induced by p53 restoration in other models[7–9], p53 restoration had no macroscopically evident impact on these tumours (Fig. 1b). Close inspection, however, indicated that p53 restoration did elicit a modest decrease in proliferating tumour cells (Fig. 1c; 14% Ki67 positive cells per Tam-treated tumours versus 21% in controls) and an increase in apoptosis (Supplementary Fig. 2 and Fig. 1d; 45% of p53-restored tumours contain apoptotic cells versus 13.5% of control tumours). Nevertheless, the distribution of apoptotic cells in tumours following p53 restoration was irregular and clustered (Fig. 1e). This high variability in the response to sustained p53 restoration was confirmed by micro-computed tomography imaging of individual tumours over 7 days. Whereas all control tumours grew during treatment, individual Tam-treated tumours showed all possible responses—some grew, others were unchanged, and many shrank (Fig. 2a and Supplementary Fig. 3). Such variability in tumour response to Tam might reflect heterogeneities among tumour cells in the efficiency of p53 restoration, in the presence of p53-activating signals, or in the engagement of downstream effectors following p53 restoration. To determine which, we first ascertained the efficiency with which Tam restored p53 function in tumours. Mice were treated for 7 days with Tam or vehicle and then exposed to a single dose of γ-radiation 2 h after the last treatment to activate p53 directly. p53 activity was then monitored in individual tumours by assaying induction of the prototypical p53-responsive gene, *CDKN1A* (*p21^{cip1}*)[16,17]. All tumours showed substantial *CDKN1A* induction (Fig. 2b), indicating that systemic Tam pervasively restores p53 function in all tumours. Hence, the heterogeneity of the therapeutic response to Tam is not a consequence of either variability in Tam-dependent p53 restoration or in the capacity of p53, once

[1]University of California San Francisco, Department of Pathology and Helen Diller Family Comprehensive Cancer Center, San Francisco, California 94143-0502, USA. [2]Cancer Research UK Cambridge Research Institute, Li Ka Shing Centre, Robinson Way, Cambridge CB2 ORE, UK. [3]University of California San Francisco, Department of Radiology and Biomedical Imaging and Helen Diller Family Comprehensive Cancer Center San Francisco, California 94143, USA. †Present addresses: Cancer Research UK Cambridge Research Institute, Li Ka Shing Centre, Robinson Way, Cambridge CB2 ORE, UK (C.P.M.); Department of Biochemistry, Tennis Court Road, University of Cambridge, Cambridge CB2 1GA, UK (G.I.E.); Department of Molecular Biology, Genentech. Inc. South San Francisco, CA 94080 , USA (M.R.J.).

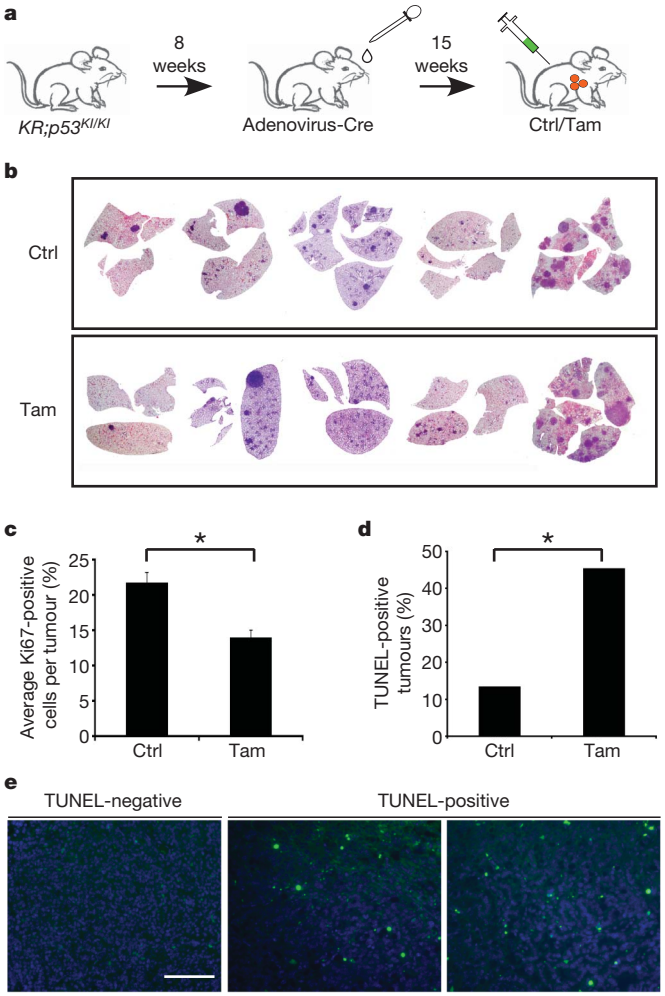

Figure 1 | Heterogeneous therapeutic impact of p53 restoration in Kras^{G12D}-driven lung tumours. **a**, Schematic representation of the experimental treatment regime. Kras^{G12D} was activated in the lung epithelium of 8-week-old *KR;p53*$^{KI/KI}$ mice by adenoviral-Cre nasal inhalation and the resulting tumours treated with Tam or vehicle (Ctrl) 15 weeks after adenoviral infection. **b**, Haematoxylin and eosin staining of lung sections from *KR;p53*$^{KI/KI}$ mice showing tumour load after 7-day control (Ctrl) or Tam treatments. **c**, Quantification of Ki67-positive cells per lung tumour from 7-day Tam/Ctrl-treated *KR;p53*$^{KI/KI}$ mice. Error bars indicate standard error of mean (Ctrl: s.e.m = 1.20 $n = 55$; Tam: s.e.m = 1.31 $n = 37$). *$P = 0.0003$, Student's *t*-test. **d**, Per cent of apoptotic (transferase dUTP nick-end labelling (TUNEL)-positive) tumours (scored as a minimum of one positive cell per tumour section) in 7-day Ctrl- and Tam-treated *KR;p53*$^{KI/KI}$ lungs ($n = 37$ Ctrl; $n = 22$ Tam-treated tumours). *$P = 0.0064$, Pearson Chi square. **e**, *KR;p53*$^{KI/KI}$ lung tumours treated for 6 h with Tam, showing either no discernible TUNEL staining (negative) or significant levels of TUNEL staining (positive). Scale bar, 100 μm.

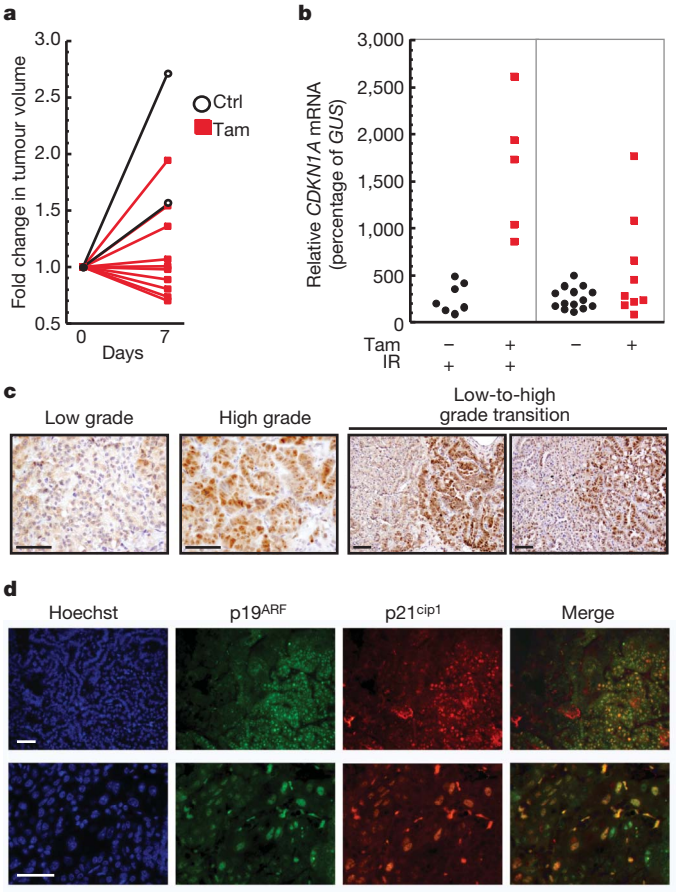

Figure 2 | Heterogeneous p53 activation and p19^{ARF} upregulation in *KR;p53*$^{KI/KI}$ tumours. **a**, Micro-computer-tomography-derived plots depicting changes in tumour volume during a 7-day treatment. Ten independent tumours are shown before (day 0) and after (day 7) daily Tam (red lines, filled symbols) or sham (black lines, open symbols) treatments. **b**, TaqMan analysis of *CDKN1A* expression in individual laser microdissected lung tumours from *KR;p53*$^{KI/KI}$ mice treated for 7 days with vehicle (black circles) or Tam (red squares). Tumours were collected 24 h after the final Ctrl/Tam treatment. Where indicated (IR +, left panel) mice were exposed to a single dose of γ-radiation 2 h after the last Tam/Ctrl treatment. Each circle/square represents a single tumour. **c**, IHC data comparing levels of p19^{ARF} expression in low- and high-grade tumours as well as in transitional lesions exhibiting both low- and high-grade features. Scale bars, 50 μm. **d**, Co-immunostaining for p19^{ARF} and p21^{cip1} in *KR;p53*$^{KI/KI}$ lung tumours from mice treated for 6 h with Tam. Representative fields shown, one at low (upper panel) and one at high magnification (lower panel). Scale bar, 50 μm.

activated, to induce *CDKN1A*. By contrast, when p53 function was restored in the absence of concomitant DNA damage, *CDKN1A* was induced in only a minority of tumours (Fig. 2b). Hence, the variability in response to p53 restoration is because only a minority of tumours harbour endogenous p53-activating signals. Interestingly, whereas we see significant apoptosis in aggressive tumour cells following p53 restoration, other researchers do not, as described in the accompanying paper[18], even though their mouse lung tumour model driven by spontaneous, sporadic Kras activation is ostensibly similar to ours. The reasons for this are unclear. However, the models differ in several ways. First, the mechanism of Kras activation is different, and may target distinct cell lineages with innately different sensitivities to p53-induced apoptosis. Second, they use Cre-*lox* recombination to restore p53 function, which is innately less synchronous than in our *p53ER*^{TAM} model and may make it difficult to see a transient wave of cell death. Cre-*lox* recombination may also introduce additional genotoxic stresses that further modify p53 output. In the end, however, whether apoptosis or arrest is the principal output of p53 restoration in aggressive tumour cells may not be so important because both p53-induced apoptosis[7] and arrest[9] are effective at eliciting tumour clearance.

Although p53 may be activated by a wide-range of stress signals, recent *in vivo* studies implicate induction of p19^{ARF} by oncogenic signalling as the critical p53-activating trigger in established tumours[7,10]. Because oncogenic Ras can be a potent inducer of p19^{ARF} (ref. 19), we assayed for p19^{ARF} expression in *KR;p53*$^{KI/KI}$ lung tumours. Immunohistochemical analysis (IHC) of *KR;p53*$^{KI/KI}$ lungs revealed p19^{ARF} expression to be highly heterogeneous—generally limited to specific regions of certain tumours. Stratification of lung tumours into low- and high-grade, the latter comprising mostly adenocarcinomas (Supplementary Fig. 4)[20], revealed that p19^{ARF} was confined mostly to high-grade tumours. High p19^{ARF} cells were only rarely

observed in low-grade tumours and, when present, were restricted to small, sporadic foci. Close examination of transitional tumours comprising clearly defined high- and low-grade regions showed $p19^{ARF}$ to be highly expressed only in high-grade/carcinoma areas (Fig. 2c).

Because $p19^{ARF}$ is a potent activator of p53, we next ascertained whether the high-grade regions expressing elevated $p19^{ARF}$ coincide with those that spontaneously activate p53 following restoration. p53 function was acutely restored in *KR;p53*$^{KI/KI}$ mice and tumours analysed for expression of $p19^{ARF}$ and $p21^{cip1}$. Upon p53 restoration, tumour areas positive for $p19^{ARF}$ overlapped extensively with those positive for $p21^{cip1}$ (Fig. 2d): ~70% of $p19^{ARF}$-positive cells from Tam-treated mice stained positive for $p21^{cip1}$ compared with 2% of control. That $p19^{ARF}$ has a causal role in engaging p53-mediated tumour suppression in high-grade tumours was corroborated by the rapid cessation of cell proliferation specific to $p19^{ARF}$-positive regions following p53 restoration (Fig. 3a, Tam, two top rows). By contrast, proliferation remained high in $p19^{ARF}$-negative tumours after p53-restoration (Fig. 3a, Tam, two bottom rows). Of note, no γ-H2AX-staining DNA damage foci were detected in *KR;p53*$^{KI/KI}$ lung tumours, although they were readily evident in tumours from γ-irradiated mice (Supplementary Fig. 5). This, together with the remarkable overlap between p53 activation and $p19^{ARF}$ expression, strongly implicates $p19^{ARF}$, and not DNA damage, as the endogenous signal responsible for triggering p53 in high-grade lung tumours.

Although germ-line *p53* deficiency significantly accelerates lung tumour progression and malignancy in *KR* mice[15], our data indicate that p53 tumour suppression acts only at later stages of tumour evolution. Since p53 is specifically activated in the most atypical tumour cells, its restoration in a mixed tumour population should lead to a shift downwards in assigned tumour grade. Indeed, 7 days of p53 restoration

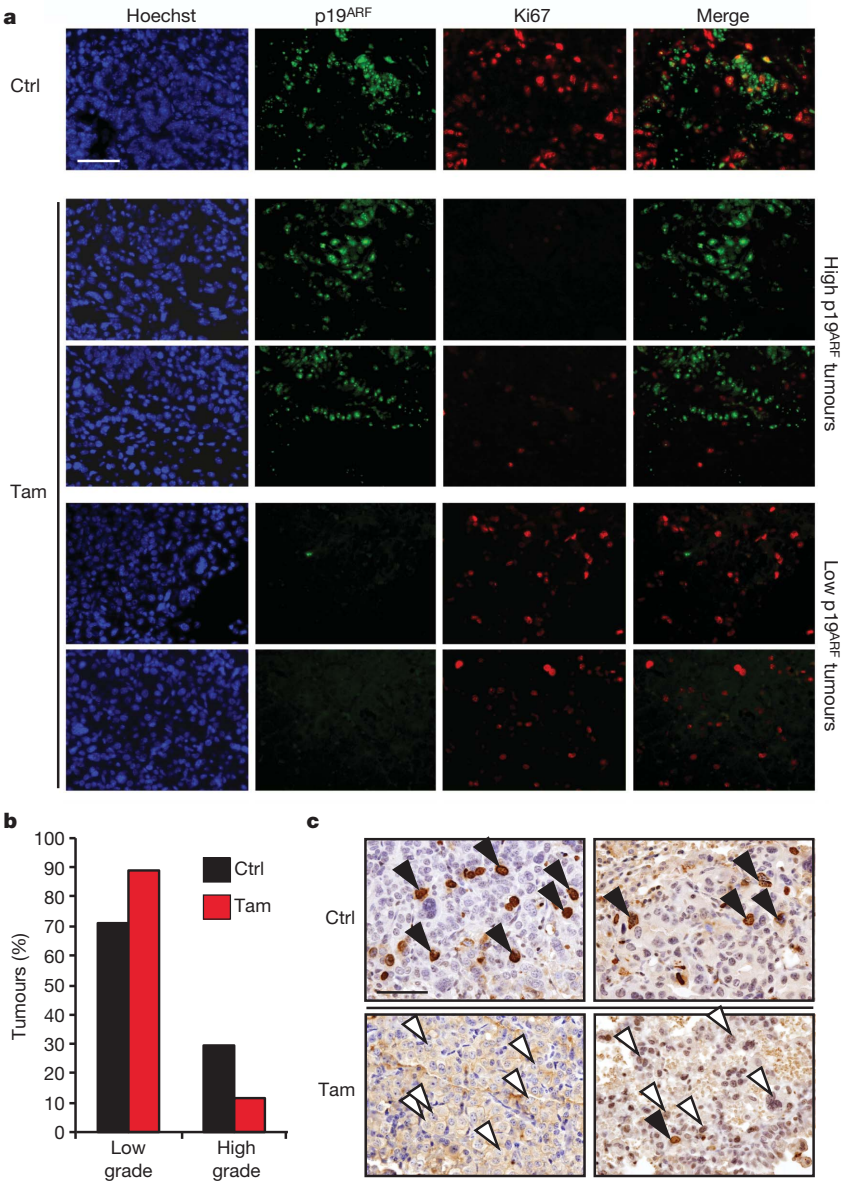

Figure 3 | p53 restoration targets high-grade, but not low-grade, lung tumour cells. **a**, Co-immunostaining for $p19^{ARF}$ and the proliferation marker Ki67 in lung tumours from *KR;p53*$^{KI/KI}$ mice treated for 24 h with vehicle (Ctrl, upper row) or Tam (four lower rows). Rows 2 and 3 illustrate the profound anti-proliferative impact (low Ki67) of p53 restoration in tumours with high $p19^{ARF}$ levels. By contrast, the lower two rows show lack of growth inhibition following p53 restoration in tumours lacking detectable $p19^{ARF}$. Scale bar, 50 μm. **b**, Quantification of low- versus high-grade tumour frequencies in lungs of *KR;p53*$^{KI/KI}$ mice treated for 7 days with either vehicle (Ctrl) or Tam ($n = 143$ Ctrl; $n = 163$ Tam). $P = 0.0001$, Pearson Chi square. **c**, Representative images show IHC for BrdU in high-grade tumours from 7-day treated Ctrl (upper panel) or Tam mice (lower panel). BrdU was administered 2 h before collection. Arrows highlight high-grade cells in each tumour (filled, BrdU-positive and open, BrdU-negative). Scale bars, 50 μm.

in *KR;p53*$^{KI/KI}$ mice harbouring a mixture of low- and high-grade tumours elicited a downward shift in the frequency of high-grade tumours (from 29% to 11%) and a *pro rata* increase in the proportion of low-grade tumours (from 71% to 89%) (Fig. 3b and Supplementary Fig. 6). The percentage of bromodeoxyuridine (BrdU)-positive high-grade cells was also markedly reduced following treatment (Fig. 3c).

Our data show that the p19^{ARF}/p53 pathway is only engaged in high-grade *KR;p53*$^{KI/KI}$ cells, even though all tumour cells harbour oncogenic Kras^{G12D}. Hence, oncogenic activity of Kras is not alone sufficient to induce p19^{ARF} and engage p53-mediated tumour suppression. Interestingly, recent *in vivo* studies indicate that intrinsic tumour suppression is only engaged when oncogenic signals are preternaturally elevated[11,12]. Such observations echo *in vitro* data showing that expression of oncogenic Kras^{G12D} from its endogenous promoter induces proliferation and immortalization, whereas Kras^{G12D} overexpression engages p53-dependent replicative senescence[21,22]. Because marked upregulation of the MAPK-pathway is a characteristic feature of advanced lung tumours in both mice[15] and NSCLC in humans[23], we asked whether induction of p19^{ARF} in high-grade tumours is a consequence of elevated flux through the Ras signalling network. Indeed, immunostaining showed a remarkably tight spatial concordance of tumour cells exhibiting elevated ERK phosphorylation (p-ERK), a signature of downstream Ras signalling, and those with high p19^{ARF} (Fig. 4a and Supplementary Fig. 7); the cell-by-cell overlap between upregulation of p19^{ARF} and p-ERK was 91.2% ($n = 1312$; s.d. = 3.77). Hence, increased flux through oncogenic Kras^{G12D} is the probable mechanism for both malignant progression and concomitant activation of (and eventual counter-selection against) the p19^{ARF}/p53 tumour suppressor pathway.

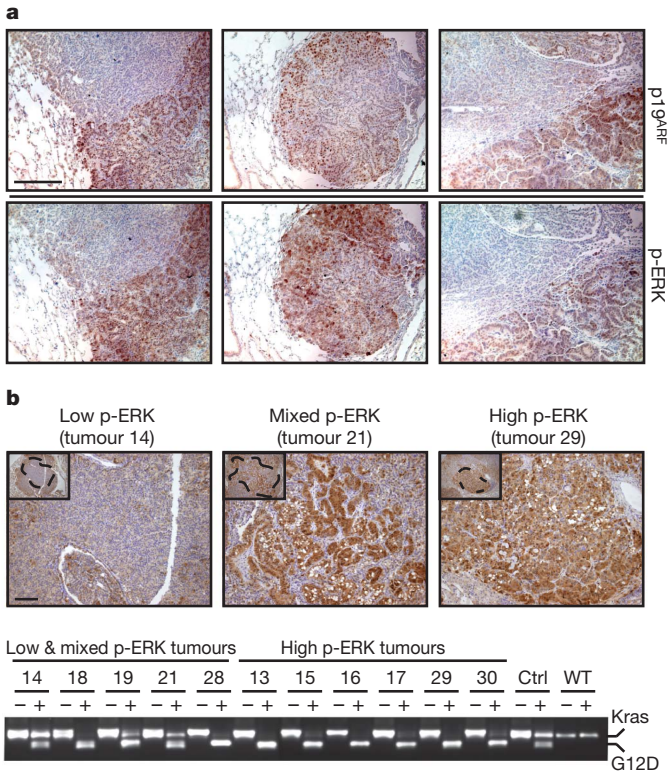

Figure 4 | High-grade lung tumours exhibit increased Kras signalling. **a**, IHC for p19^{ARF} and p-ERK in consecutive sections of three independent low-to-high-grade transition tumours from *KR;p53*$^{KI/KI}$ mice. Scale bar, 200 μm. **b**, *Kras* allele analysis was performed on genomic DNA from *KR;p53*$^{KI/KI}$ lung tumours following laser microdissection. p-ERK IHC was used to define areas of low, mixed or high p-ERK (upper panel, scale bar, 50 μm) and consecutive slides used for LCM of defined regions (see dotted areas). DNA was isolated from LCM material and the *Kras* genomic region amplified by PCR and digested with HindIII (lower panel). For each tumour, the undigested (−) and digested (+) PCR fragments were run alongside and the wild-type (*Kras,* higher band) and mutant alleles (G12D, lower band) are indicated. Control lung tissue from heterozygous (Kras$^{G12D/+}$: Ctrl) and wild-type (WT) mice was also analysed.

Many potential mechanisms might underlie the dramatic upregulation of p-ERK we observe in high-grade lung tumours, including changes in *Kras* copy number (known to occur in human NSCLC), inactivation of Kras negative feedback mechanisms and incidental activation of cooperating oncogenes[24–27]. Initial analysis of whole low- versus high-grade tumours indicated downregulation of Sprouty 2 (also known as Spry2) or loss of the wild-type *Kras* allele as possible mechanisms for Kras signal upregulation in high p-ERK tumours (Supplementary Fig. 8). Because elevated Ras signalling is a property peculiar to high-grade tumour regions, we used p-ERK staining to demarcate high, low and mixed p-ERK areas of individual tumours (Fig. 4b, upper panel). These tumour regions were individually laser microdissected and their genomic DNA extracted and assessed for the relative copy representation of wild-type versus mutant *Kras* alleles. We saw variable levels of wild-type *Kras* retention in the low/mixed p-ERK tumour tissues, ranging from 100% in the low p-ERK tumour 14 to partial or total loss in the mixed grade tumours (for example, 21 and 18). Remarkably, the wild-type *Kras* allele was lost in all high p-ERK tumours (Fig. 4b, lower panel) and the mutant *Kras* allele often duplicated (Supplementary Fig. 9). Overall, across all tumour samples *Kras* allelic imbalance, a known mechanism by which Ras signal strength is elevated[27], correlated tightly with high p-ERK.

Long-lived organisms must solve the problem of suppressing cancer without compromising the facility of normal cells to proliferate. This requires an accurate means of distinguishing between normal and oncogenic signals. However, emerging evidence hints at a 'flaw' in how our tumour suppressor pathways have evolved—rather than responding to the aberrant signal persistence that is actually responsible for oncogenesis, mammalian intrinsic tumour suppressor pathways have instead evolved to respond to the unusual elevation in signal intensity that often (but not invariably) accompanies oncogenic activation[11]. Paradoxically, therefore, low-level oncogenic activities may be more efficient at initiating tumorigenesis than high-level oncogenic signals because they 'fall beneath the radar' of tumour surveillance[28]: high-level oncogenic signals, which seem necessary to drive progression to malignancy, are tolerable only once p53 function has been quelled.

At first glance, our data showing limited therapeutic impact of restoring p53 in established lung tumours seem at odds with previous studies[7–9]. However, such studies used advanced, relatively homogenous tumours driven by high levels of oncogenic signalling that had already engaged the ARF pathway—hence the dramatic impact of re-instating p53. By contrast, the spontaneously evolving lung tumours that afflict *KR* mice are initiated by sporadic oncogenic activation of endogenous Kras at a level insufficient to engage p53. Our data indicate that it is only relatively late in their evolution, at the point when sporadic elevation of Ras signalling precipitates tumours into aggressive, high-grade lesions, that the p53 pathway is triggered. Such considerations offer a compelling rationale for the long-baffling observation that selection for p53 pathway inactivation arises relatively late in the evolution of many solid human tumours.

The inability of low-level oncogenic signalling to engage p53 also casts a cautionary shadow over the potential efficacy of p53 restoration in treating cancer. Established tumours are typically comprised of heterogeneous clades of neoplastic clones that encompass all phases of oncogenic evolution. Although p53 restoration might cull the most malignant cells, less aggressive tumour cells driven by low-level oncogenic signals would presumably survive to evolve another day. At best, then, p53 restoration as a single therapy would be a means of temporary tumour containment rather than eradication.

METHODS SUMMARY

Tumour induction and treatment. Animals were maintained under UCSF IACUC-approved protocols. *KR*[5] and p53^{KI} mice[14] progeny were infected with adenovirus-CRE (5×10^7 plaque-forming units (p.f.u.) per mouse) by nasal inhalation at 8 weeks of age[5]. p53 function was restored by intraperitoneal injection of tamoxifen (1 mg per mouse daily)[7,10,14]. Where appropriate, mice were irradiated (4 Gy) 2 h after Ctrl/Tam treatment using a Mark 1-68 ^{137}Cs source (0.637 Gy min^{-1}). A minimum of five mice per cohort was used for each experiment.

Immunohistochemistry and immunofluorescence. Primary antibodies used were p19^{ARF} (gift from C. J. Sherr and M. F. Roussel[29]); p21 (BD Pharmingen #556430); Ki67 (SP6 Neomarkers); P-ERK (Cell Signaling Technologies #4376) and phospho-histone H2AX (Upstate #05-636). They were detected with horseradish peroxidase-/Alexa-conjugated secondary antibodies. An ApopTag kit (Millipore) was used for terminal deoxynucleotidyl transferase dUTP nick-end labelling (TUNEL).

Laser capture microdissection, expression and copy number analysis. For *CDKN1A* TaqMan analysis[7], laser capture microdissection of frozen samples[30] was followed by RNA preparation (Arcturus PicoPure RNA Isolation kit, Arcturus Engineering) and cDNA production (iScript cDNA Synthesis kit, Bio-Rad). For copy number analysis, laser microdissection (Zeiss P.A.L.M.) collection of paraffin samples was followed by DNA isolation (QIAamp DNA Micro kit #56304) and TaqMan (probes: β-actin: Mm00607939_s1; Kras: Mm03053281_s1, Applied Biosystems) or PCR (primers: KrasHind3_F 5′-GCCATTAGCTGCTACAAA ACAGTA-3′ and KrasHind3_R 5′-CCTCTATCGTAGGGTCGTACTCAT-3′). Following PCR the *Kras*^{G12D} and *Kras*^{wt} alleles were distinguished by the presence of a *Kras*^{G12D}-specific HindIII site in the amplified fragment (wild-type = 400 base pairs; Kras^{G12D} = 300 + 100 bp).

Micro-computed X-ray tomography. Pre- (day 0) and post-therapy (day 7) micro-computed tomography data was acquired using a FLEX X-O system (Gamma Medica-Ideas). Only clearly discrete tumours were measured.

Immunoblot analysis. Whole-cell lysates from dissected tumour halves were immunoblotted with anti-Spry2 (Abcam ab50317), anti-Dusp6 (Santa Cruz sc-28902) or anti-β-actin (Sigma A5441) antibodies.

Full Methods and any associated references are available in the online version of the paper at www.nature.com/nature.

Received 22 December; accepted 21 September 2010.

1. Jemal, A. *et al.* Cancer statistics, 2006. *CA Cancer J. Clin.* **56,** 106–130 (2006).
2. Meuwissen, R. & Berns, A. Mouse models for human lung cancer. *Genes Dev.* **19,** 643–664 (2005).
3. Serrano, M., Lin, A., McCurrach, M., Beach, D. & Lowe, S. Oncogenic *ras* provokes premature cell senescence associated with accumulation of p53 and p16^{INK4a}. *Cell* **88,** 593–602 (1997).
4. Wang, W. & El-Deiry, W. S. Restoration of p53 to limit tumor growth. *Curr. Opin. Oncol.* **20,** 90–96 (2008).
5. Jackson, E. L. *et al.* Analysis of lung tumor initiation and progression using conditional expression of oncogenic *K-ras*. *Genes Dev.* **15,** 3243–3248 (2001).
6. Kamijo, T. *et al.* Tumor suppression at the mouse *INK4a* locus mediated by the alternative reading frame product p19^{ARF}. *Cell* **91,** 649–659 (1997).
7. Martins, C. P., Brown-Swigart, L. & Evan, G. I. Modeling the therapeutic efficacy of p53 restoration in tumors. *Cell* **127,** 1323–1334 (2006).
8. Ventura, A. *et al.* Restoration of p53 function leads to tumour regression *in vivo*. *Nature* **445,** 661–665 (2007).
9. Xue, W. *et al.* Senescence and tumour clearance is triggered by p53 restoration in murine liver carcinomas. *Nature* **445,** 656–660 (2007).
10. Christophorou, M. A., Ringshausen, I., Finch, A. J., Swigart, L. B. & Evan, G. I. The pathological response to DNA damage does not contribute to p53-mediated tumour suppression. *Nature* **443,** 214–217 (2006).
11. Murphy, D. J. *et al.* Distinct thresholds govern Myc's biological output *in vivo*. *Cancer Cell* **14,** 447–457 (2008).
12. Sarkisian, C. J. *et al.* Dose-dependent oncogene-induced senescence *in vivo* and its evasion during mammary tumorigenesis. *Nature Cell Biol.* **9,** 493–505 (2007).
13. Sweet-Cordero, A. *et al.* An oncogenic *KRAS2* expression signature identified by cross-species gene-expression analysis. *Nature Genet.* **37,** 48–55 (2005).
14. Christophorou, M. A. *et al.* Temporal dissection of p53 function *in vitro* and *in vivo*. *Nature Genet.* **37,** 718–726 (2005).
15. Jackson, E. L. *et al.* The differential effects of mutant p53 alleles on advanced murine lung cancer. *Cancer Res.* **65,** 10280–10288 (2005).
16. Dulić, V. *et al.* p53-dependent inhibition of cyclin-dependent kinase activities in human fibroblasts during radiation-induced G1 arrest. *Cell* **76,** 1013–1023 (1994).
17. El Deiry, W. S. *et al. WAF1/CIP1* is induced in *p53*-mediated G_1 arrest and apoptosis. *Cancer Res.* **54,** 1169–1174 (1994).
18. Feldser, D. *et al.* Stage-specific sensitivity to p53 restoration in lung cancer. *Nature* doi:10.1038/nature09535 (in the press).
19. Palmero, I., Pantoja, C. & Serrano, M. p19^{ARF} links the tumour suppressor p53 to Ras. *Nature* **395,** 125–126 (1998).
20. Nikitin, A. Y. *et al.* Classification of proliferative pulmonary lesions of the mouse: recommendations of the mouse models of human cancers consortium. *Cancer Res.* **64,** 2307–2316 (2004).
21. Guerra, C. *et al.* Tumor induction by an endogenous *K-ras* oncogene is highly dependent on cellular context. *Cancer Cell* **4,** 111–120 (2003).
22. Tuveson, D. A. *et al.* Endogenous oncogenic *K-ras(G12D)* stimulates proliferation and widespread neoplastic and developmental defects. *Cancer Cell* **5,** 375–387 (2004).
23. Vicent, S. *et al.* ERK1/2 is activated in non-small-cell lung cancer and associated with advanced tumours. *Br. J. Cancer* **90,** 1047–1052 (2004).
24. Shaw, A. T. *et al.* Sprouty-2 regulates oncogenic K-ras in lung development and tumorigenesis. *Genes Dev.* **21,** 694–707 (2007).
25. Wagner, P. L. *et al. In situ* evidence of *KRAS* amplification and association with increased p21 levels in non-small cell lung carcinoma. *Am. J. Clin. Pathol.* **132,** 500–505 (2009).
26. Zhang, Z. *et al.* Dual specificity phosphatase 6 (DUSP6) is an ETS-regulated negative feedback mediator of oncogenic ERK signaling in lung cancer cells. *Carcinogenesis* **31,** 577–586 (2010).
27. Zhang, Z. *et al.* Wildtype *Kras2* can inhibit lung carcinogenesis in mice. *Nature Genet.* **29,** 25–33 (2001).
28. Junttila, M. R. & Evan, G. I. p53 – a Jack of all trades but master of none. *Nature Rev. Cancer* **9,** 821–829 (2009).
29. Bertwistle, D., Zindy, F., Sherr, C. J. & Roussel, M. F. Monoclonal antibodies to the mouse p19^{Arf} tumor suppressor protein. *Hybrid. Hybridomics* **23,** 293–300 (2004).
30. Lawlor, E. R. *et al.* Reversible kinetic analysis of Myc targets *in vivo* provides novel insights into Myc-mediated tumorigenesis. *Cancer Res.* **66,** 4591–4601 (2006).

Supplementary Information is linked to the online version of the paper at www.nature.com/nature.

Acknowledgements We are indebted to T. Jacks for the *KR* mice, C. Sherr and M. Roussel for the p19^{ARF} antibody, M. Dail and A.-T. Maia for advice on *Kras* copy number analysis and V. Weinberg for guidance on statistical analysis. We also thank D. Tuveson and all the members of the Evan laboratory for their comments. This work was supported by grants NCI CA98018, NCI CA100193, AICR 09-0649, the Ellison Medical Foundation and from the Samuel R. Waxman Cancer Research Foundation (all to G.I.E.). M.R.J. is the Enrique Cepero, PhD Fellow of the Damon Runyon Cancer Research Foundation.

Author Contributions C.P.M. and G.I.E. designed this study with help from M.R.J. C.P.M. and M.R.J. performed all experiments with assistance from D.G. and F.M. C.P.M., M.R.J. and G.I.E. analysed and interpreted the data. A.N.K. graded all tumours. L.B.S., F.R. and R.M.K. helped maintain the mouse colony. D.M.P. and Y.S. performed the micro-computed tomography analysis. C.P.M. and G.I.E. wrote the paper with help from M.R.J. and all authors contributed to editing.

Author Information Reprints and permissions information is available at www.nature.com/reprints. The authors declare no competing financial interests. Readers are welcome to comment on the online version of this article at www.nature.com/nature. Correspondence and requests for materials should be addressed to G.I.E. (gie20@cam.ac.uk).

METHODS

Mice, adenoviral infection and treatments. Animals were maintained in SPF conditions under UCSF IACUC-approved protocols. *KP*[5] and p53^{KI} mice[14] were crossed and *KP* and *KP*;p53$^{KI/KI}$ animals were infected by nasal inhalation with adenovirus-CRE (5×10^7 plaque-forming units per mouse) at 8 weeks of age, as described[5]. p53 function was restored by treating mice with tamoxifen (1 mg per mouse daily) delivered by intraperitoneal injection, as described[7,10,14]. Where appropriate, mice were irradiated (4 Gy) 2 h after Ctrl/Tam treatment using a Mark 1-68 ^{137}Cs source (0.637 Gy min^{-1}). A minimum of five mice per cohort were used for each experiment.

Immunohistochemistry and immunofluorescence. IHC stainings were performed on z-fix fixed, 5-μm paraffin-embedded tissue sections. Sections were incubated overnight at 4 °C with the following primary antibodies: p19^{ARF} (gift from C. J. Sherr and M. F. Roussel[29]); p21 (BD Pharmigen #556430); Ki67 (SP6, Neomarkers); P-ERK (Cell Signaling Technologies #4376), phospho-histone H2AX (Upstate #05-636). Antibodies were detected using Vectastain ABC detection (Vector Laboratories) or with specific biotinylated secondary antibodies (anti-rat biotinylated, Vector Laboratories BA-4001 and anti-rabbit biotinylated, Dako #E0432) followed with stable diaminobenzidine treatment (Invitrogen). Alternatively, Alexa-conjugated mouse, rat or rabbit IgG antibodies were used (Molecular Probes). TUNEL staining was performed using the ApopTag fluorescein labelled kit (Millipore) according to the manufacturer's directions.

Laser capture microdissection, expression and copy number analysis. For RNA analysis 30-μm sections from fresh frozen lung tissue were fixed, stained and laser microdissected, as described previously[30]. Total RNA was isolated and DNase I treated using the Arcturus PicoPure RNA Isolation kit (Arcturus Engineering). cDNA was produced using iScript cDNA Synthesis kit (Bio-Rad). Real-time quantitative PCR (qPCR) was performed as described previously[7]. For copy number analysis 5-μm sections were briefly de-paraffinized and laser microdissected using a Zeiss P.A.L.M. LCM microscope. Genomic DNA was isolated using the QIAamp DNA Micro Kit #56304 and analysed by TaqMan or PCR. Copy number TaqMan analysis was carried out using the following probes from Applied Biosystems: β-actin: Mm00607939_s1; Kras: Mm03053281_s1. PCR was performed using the following Kras-specific primers: KrasHind3_F 5′-GCCA TTAGCTGCTACAAAACAGTA-3′ and KrasHind3_R 5′-CCTCTATCGTA GGGTCGTACTCAT-3′. Due to the presence of a unique HindIII restriction site in the *Kras*^{G12D} allele, the mutant and wild-type alleles can be distinguished based on their HindIII restriction-digestion profile (wild type = 400 bp and Kras^{G12D} = 300 + 100 bp).

Micro-computed X-ray tomography. Computed tomography (CT) was performed using a micro CT system (FLEX X-O, Gamma Medica-Ideas) with an X-ray source with 75 kVp (kilovolts peak) and 0.315 mA. CT data were acquired as 512 projections over 120 s of continuous X-ray exposure. Pre-therapy CT data were acquired as the baseline time point and post-therapy CT performed after 7 days of sustained Tamoxifen administration. Only clearly discrete tumours were picked for volume measurements. Volumes of interest were drawn on axial slices, and the total tumour volumes were calculated planimetrically.

Immunoblot analysis. Whole-cell lysates from dissected tumour halves were prepared and immunoblotted with anti-Spry 2 (Abcam ab50317), Dusp6 (Santa Cruz sc-28902) or β-actin (Sigma A5441) antibodies.